Magnetostrictive Néel ordering of the spin-$\frac{5}{2}$ ladder compound $BaMn_2O_3$: Distortion-induced lifting of geometrical frustration

M. Valldor,[1] O. Heyer,[1] A. C. Komarek,[1] A. Senyshyn,[2] M. Braden,[1] and T. Lorenz[1]
[1]*II. Physikalisches Institut, Universität zu Köln, Zülpicher Str. 77, DE-50937 Köln, Germany*
[2]*Technische Universität Darmstadt, Material und Geowissenschaften, Petersenstr. 23, DE-64287 Darmstadt, Germany and Technische Universität München, FRM-II, Lichtenbergstr. 1, DE-85747 Garching, Germany*
(Received 6 October 2010; revised manuscript received 6 December 2010; published 31 January 2011)

The crystal structure and the magnetism of $BaMn_2O_3$ have been studied by thermodynamic and diffraction techniques using large single crystals and powders. $BaMn_2O_3$ is a realization of an $S = \frac{5}{2}$ spin ladder as the magnetic interaction is dominant along 180° Mn–O–Mn bonds forming the legs and the rungs of a ladder. The temperature dependence of the magnetic susceptibility exhibits well-defined maxima for all directions, proving the low-dimensional magnetic character in $BaMn_2O_3$. The susceptibility and neutron powder diffraction data, however, show that $BaMn_2O_3$ exhibits a transition to antiferromagnetic order at 184 K, in spite of a full frustration of the nearest-neighbor interladder coupling in the orthorhombic high-temperature phase. This frustration is lifted by a remarkably strong monoclinic distortion, which accompanies the magnetic transition.

DOI: 10.1103/PhysRevB.83.024418 PACS number(s): 75.10.Jm, 75.40.Cx, 75.80.+q

I. INTRODUCTION

Exotic magnetic ground states are expected and have been observed in a special group of layered metal oxides containing spin ladders.[1–5] Up until now, such ladder systems have been mainly studied in cuprates, where the quasi-one-dimensional (1D) magnetic units are built by $S = \frac{1}{2}$ ($3d^9$) Cu^{2+} ions, which are typically connected via O^{2-} ions; see, e.g., Refs. 6 and 7. One prominent example is the ladder-chain system $(Sr,Ca)_{14}Cu_{24}O_{41}$ that belongs to the most well-studied spin liquids and does not evolve long-range magnetic order at finite temperatures. This mainly arises from a very effective magnetic decoupling of neighboring spin ladders as a result of a geometrical frustration of the magnetic spin interactions, which is present between the ladders. The strongest antiferromagnetic (AFM) spin-spin couplings J_1 and J_2 are expected, respectively, along the rungs and legs of the spin ladders due to almost perfect super-exchange conditions,[8,9] which are responsible for interesting spin dynamics.[10] Small anisotropies in J within the ladders could also result in spin dimerization.[11] Furthermore, because of the low dimensionality of such spin-ladder materials, they can act as model systems and connect theory with experiment in, e.g., spectroscopy,[12–15] thermal conductivity,[16,17] and thermodynamics.[18,19] The spin-ladder structural features are still rare in nature, but are present in the metal oxide $BaMn_2O_3$.[20] The high spin moment $S = \frac{5}{2}$ of Mn^{2+} ($3d^5$) represents a very different situation as for the cuprates, but theoretical work on the $S = \frac{5}{2}$ model systems predicts dimerization.[21] Here, we present a combined study of magnetism, x-ray and neutron diffraction, and thermodynamic properties on $BaMn_2O_3$.

The room-temperature crystal structure of $BaMn_2O_3$ has been described by Sander and Müller-Buschbaum[20] and is shown in Fig. 1(a). Similar to the hexagonal $RMnO_3$ (R = Ho–Lu, Sc, and Y),[22] Mn has a five-fold coordination, which forms an almost perfect trigonal bipyramid. However, the relatively lower oxygen content in $BaMn_2O_3$, i.e., the lower oxidation state of Mn, forces the MnO_5 polyhedra to also share edges instead of only corners. This condensation is known as shear planes in tungstenates[23] and causes the structure to evolve double layers of edge-sharing MnO_5 polyhedra, perpendicular to the b axis, with corner sharing as the only connection between these double layers. The Ba^{2+} ions fill the space between the layers and coordinate eight oxygen ions. The Mn–O–Mn super exchange, however, is not governed by the double layers but by the bond angles and the bond directions, shown in Fig. 1(b), which amount to 180° [010], 172° [100], 112° [001], and 92.3°, which should ensure strong magnetic coupling along the rungs (J_1) and the legs (J_2) of each ladder, but weaker interactions between them. The Mn–to–Mn interactions from one ladder to the nearest-neighboring ladders constitute a complete geometric frustration. By symmetry, the interactions are equally strong to the two next-nearest Mn^{2+} ions in the nearest-neighboring ladder [thick dashed lines in Fig. 1(b)]. This results in a geometric frustration and in an effective decoupling of the neighboring ladders, and quasi-1D AFM interactions along the [100] axis are expected to dominate the magnetic correlations of $BaMn_2O_3$.

II. EXPERIMENTAL

A single crystal of centimeter size was synthesized using a floating-zone image furnace (FZ-T-10000-H-VI-VP) in a flowing gas mixture of N_2/H_2(5%) (0.25 dm^3/min). Both feeding bar and seed were pressed from stoichiometric amounts of $BaCO_3$ (Strem Chem. 99.9%) and MnO (Aldrich 99%). The issue of BaO loss due to a transport reaction with H_2 (as was mentioned in the first paper on this compound)[20] could, to some extent, be avoided by growing the crystal at a relatively high rate of 10 mm/h. Indeed, the obtained crystal was covered by a thin layer of lime green crystals (MnO), indicating a small loss of BaO, but this top layer could be removed mechanically. Such a pure $BaMn_2O_3$ crystal appears dark, almost black, but thinner parts reveal that the compound is transparent and dark forest green. The pale yellow color observed in Ref. 20 can be seen if the crystals are further crushed, reaching micrometer size. The compound decomposes slowly in air, but relatively fast in water. Both reactions cause the crystal surface to become

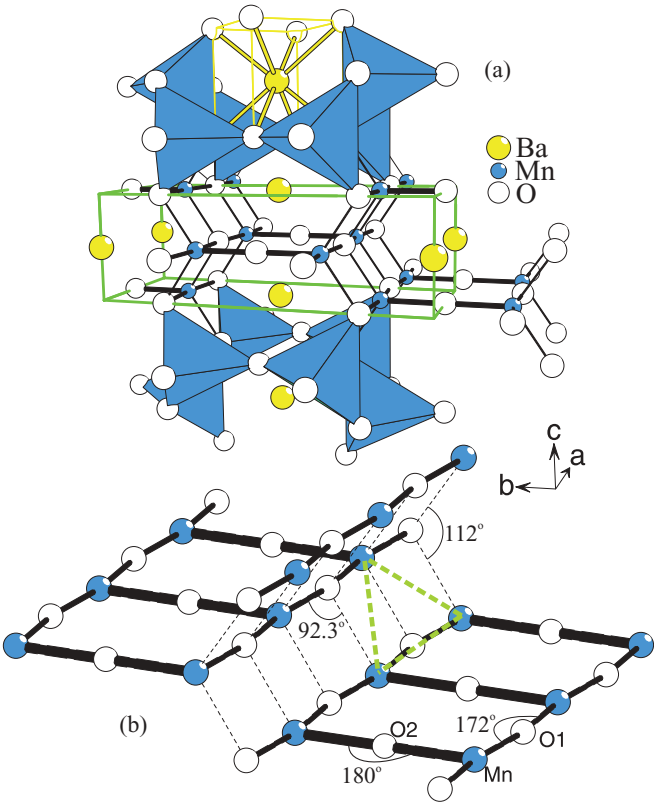

FIG. 1. (Color online) (a) Room-temperature structure of $BaMn_2O_3$. The open balls at the corners of the Mn-containing polyhedra are oxygen atoms; the closed large and small balls represent Mn and Ba ions, respectively. In addition, the unit cell is displayed by lines. (b) A selected part of the structure showing the Mn-O substructure with Mn–O–Mn bond angles. The thick dashed lines indicate the geometrical frustration, as discussed in the text.

brown, probably due to formation of Ramsdellite (α-MnO_2) and barium hydroxides and carbonates.

Elemental analysis was performed in a scanning electron microscope SEM515 (Philips) equipped with an EDX unit at 20 kV acceleration voltage. The average metal-to-metal composition was determined to be $Ba_{1.002(8)}Mn_{1.998(8)}$ from 10 EDX analyses at different spots on a centimeter-sized single-crystal slice; this very well agrees with the expected metal stoichiometry. The purity of the sample was checked by powder x-ray diffraction and no impurity phases could be detected, meaning that the sample is at least 95% pure.

The x-ray powder diffraction data were collected at 300 K using a Cr $K_{\alpha_{1,2}+\beta}$ x-ray tube ($\lambda = 2.28973$, 2.29365, and 2.08090 Å) as the source. The intensities were collected in reflection (Bragg-Brentano) geometry. Single-crystal x-ray measurements were performed down to 100 K with a Bruker X8 APEX (Mo$K_{\alpha_{1,2}}$, $\lambda = 0.7093$ and 0.71359 Å); the cooling was accomplished by using a flow of dry N_2 gas (Cryoflex). Neutron diffraction data were collected at SPODI, FRM II (Munich, Germany), with a constant wavelength of 2.537 Å (Ge [331] monochromator) at temperatures between 3 and 300 K. A vanadium cup was used as a sample holder for the powdered single-crystal sample.

Magnetic and specific-heat measurements were performed in a commercial physical-properties measurement system (PPMS, Quantum Design Inc.) in the temperature range 2–400 K in magnetic fields up to 14 T. The magnetization was measured by the vibrating-sample technique while either the magnetic field or the temperature is continuously varied. For the specific heat, a relaxation-time method is used and the data points are typically obtained stepwise after stabilizing certain temperatures. In addition, we also used a quasicontinuous modification of this relaxation-time method (see Ref. 24) in the temperature range around the first-order phase transition. Thermal expansion was investigated on a home-built high-resolution capacitance dilatometer.

To ensure that the sample did not deteriorate in air, the crystal was only handled in an Ar-filled glove box and sealed in a shrink hose before performing the magnetic measurements. For all the other methods, the crystals were rapidly transferred in air from the Ar-filled glove box to the respective measurement setups, which work either in He atmosphere, dry N_2 gas, or under vacuum conditions. There were no indications for the presence of a sizable amount of impurity phases in any of the measurements on $BaMn_2O_3$ single crystals. This was different for the neutron powder-diffraction data, which revealed that the studied sample contains about 3% of MnO. This impurity phase in the neutron data probably originates from the fact that the exposure to air is more severe for a powdered sample with a much larger surface-to-volume ratio than a single crystal.

III. THERMODYNAMIC PROPERTIES

Figure 2 summarizes the magnetic measurements. Between about 200 and 400 K, the magnetic susceptibility χ shows a weak anisotropy with respect to the direction of the applied magnetic field. The data of Fig. 2 have been obtained after cooling the sample in zero magnetic field. The corresponding data from field-cooling experiments (not shown) perfectly superimpose these data for all three field directions, which rules out the existence of ferromagnetic domains or a spin-glass behavior in $BaMn_2O_3$. For all three field directions, the temperature dependences $\chi_i(T)$ strongly deviate from a simple

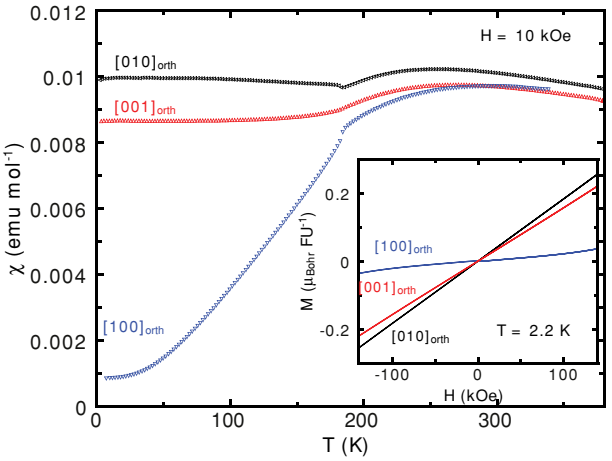

FIG. 2. (Color online) Magnetic susceptibility as a function of temperature measured in magnetic fields of 1 T applied along all three orthorhombic crystallographic directions of $BaMn_2O_3$. The inset displays magnetization curves measured at 2.2 K as a function of the magnetic field up to 14 T applied along the orthorhombic axes.

Curie-Weiss behavior. Instead, the $\chi_i(T)$ show broad maxima which, depending on the field direction i, are located between about 250 and 290 K. These broad maxima are typical for low-dimensional magnets and signal the continuous increase of magnetic correlations with decreasing temperature. The susceptibility data unambiguously prove the low-dimensional nature of magnetic correlations in $BaMn_2O_3$. At $\simeq 184$ K, clear anomalies occur in all three $\chi_i(T)$: for a field along the orthorhombic a axis, χ_a strongly decreases and levels off at a very small value at the lowest temperature, while for a field along the orthorhombic b (c) axis χ_i slightly increases (decreases) below 184 K and finally remains essentially constant below about 100 K. This anisotropic behavior is a clear indication of an antiferromagnetic ordering, where, below the Néel temperature $T_N \simeq 184$ K, the spins spontaneously align predominantly (anti)parallel to the orthorhombic a axis.

The low-temperature magnetization measured as functions of magnetic fields up to 14 T applied along these three field directions is shown in the inset of Fig. 2. Obviously, there are neither indications of metamagnetic transitions nor of a magnetic hysteresis. Instead, these data show that the low-field anisotropy observed in the temperature-dependent measurements at 1 T remains essentially preserved up to a field of 14 T. At first glance, this is a surprising observation because, for the $3d^5$ configuration of Mn^{2+}, the orbital contribution to the magnetic moment is typically small and consequently the magnetic anisotropy is expected to be weak. In other words, Mn^{2+} systems are expected to represent rather well the spin-$\frac{5}{2}$ Heisenberg system. In this case, however, only a weak magnetic anisotropy is expected and comparatively low magnetic fields along the easy a axis should be sufficient to induce a so-called spin-flop transition, where the spin orientation changes from being (anti)parallel to the a axis to a direction within the plane perpendicular to a.

A rough estimate of the effective intraladder interaction can be obtained by comparing the positions of the susceptibility maxima of $BaMn_2O_3$ to Monte Carlo simulations of $S = \frac{5}{2}$ ladders.[21] According to these simulations, the susceptibility maximum is expected to occur at $T \simeq 6.69J$ for a homogeneous spin ladder with equal rung and leg coupling $J_1 = J_2 = J$. Thus, our data suggest an intraladder coupling $J \simeq 40$ K. Due to the large spin value, this interaction corresponds to a very large saturation field $H_{\rm sat} = 2Sk_B(2J_1 + J_2)/g\mu_B \simeq 450$ T. In view of this large saturation field, the absence of a spin-flop transition in the studied field range appears less surprising, because from the present data one can only conclude that the spin-flop field $H_{\rm SF}$ is larger than 14 T, i.e., $H_{\rm SF}/H_{\rm sat} > 3$ %. According to Ref. 25, a weak anisotropy field $H_A > 10^{-3}H_{\rm sat}$ would already be sufficient to explain $H_{\rm SF} > 14$ T. A closer inspection of the data in the inset of Fig. 2 reveals a weak increase of slope in the high-field region of the magnetization curve for a field applied along a. Thus, one may speculate that a spin-flop transition could occur in the field range slightly above our maximum field. In order to clarify this issue, measurements to higher fields are necessary.

In the specific heat, shown in Fig. 3(a), a pronounced anomaly appears close to 184 K, which signals a release in entropy. The specific-heat peak is slightly asymmetric,

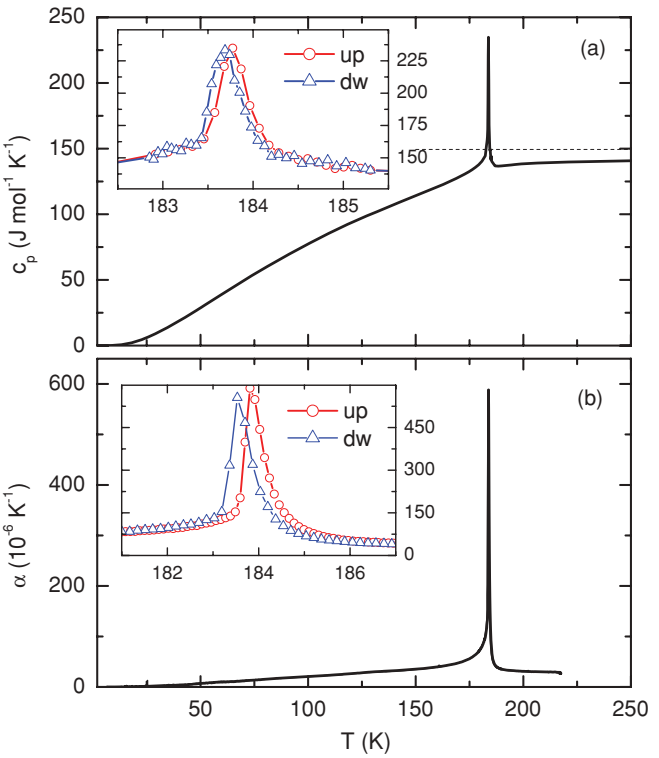

FIG. 3. (Color online) (a) Specific heat and (b) linear thermal expansion of $BaMn_2O_3$ in zero magnetic field. Thermal expansion was measured along the $[001]_{\rm orth}$ direction. The dashed line in the upper panel marks the Dulong-Petit limit. In both panels, the inset is a blow-up of the respective heating (up) and cooling (dw) curves in the temperature range close to the Néel ordering.

i.e., λ-like, which would infer that the phase transition is of second order. However, measurements with increasing and decreasing temperature reveal a small hysteresis of $\simeq 0.2$ K [inset of Fig. 3(a)], which identifies this transition as a weak first-order one. In Fig. 3(b), we show the linear thermal expansion measured along the [001] direction according to the orthorhombic settings. Again, a strong anomaly is observed close to 184 K, with a minor thermal hysteresis of about 0.2 K between the curves measured on increasing and decreasing temperature, in very good agreement with the results of the specific-heat data. The magnitude of the thermal-expansion anomaly at T_N is huge, which reveals that this magnetic ordering strongly couples to the lattice. The strong magnetoelastic coupling is also the most likely reason for the first-order nature of this phase transition. It has been shown that an intrinsically second-order phase transition can be driven to first order by a finite coupling to the lattice.[26,27]

From the presented macroscopic data, the behavior of $BaMn_2O_3$ may be summarized as follows: $BaMn_2O_3$ contains two-leg spin ladders with spin $\frac{5}{2}$ and a rather strong intraladder interaction of the order of $J \simeq 40$ K, as inferred from the broad susceptibility maxima around 270 K. Despite this large exchange coupling, a three-dimensional Néel order is suppressed because the effective interladder coupling is weak as a consequence of the geometrical arrangement of neighboring ladders that causes strong magnetic frustration. Nevertheless, $BaMn_2O_3$ undergoes an antiferromagnetic ordering transition

at $T = 184$ K. In order to allow for a three-dimensional Néel ordering, this frustration can be lifted by a structural distortion, which then naturally explains the strong magnetoelastic coupling and the weakly first-order nature of the observed phase transition at 184 K. In order to resolve the microscopic details of these structural changes and the magnetic structure, we performed single-crystal x-ray measurements down to 100 K as well as neutron powder-diffraction measurements on a crushed single crystal in the temperature range from 3 to 300 K.

IV. CRYSTALLOGRAPHIC AND MAGNETIC STRUCTURE

The structure refinement using Fullprof2k (Ref. 28) of the x-ray powder-diffraction data (not shown) of a crushed piece of the $BaMn_2O_3$ single crystal yields the unit-cell parameters $a = 4.3819(1)$ Å, $b = 10.9745(5)$ Å, and $c = 3.55329(8)$ Å, in good agreement with $a = 4.385$ Å, $b = 10.967$ Å, and $c = 3.552$ Å as reported previously.[20] Our room-temperature x-ray diffraction data perfectly agree with the already reported $Immm$ symmetry, but the low-temperature data (at 150 and 100 K) of a $BaMn_2O_3$ single crystal (see Table I) clearly indicate a lower monoclinic symmetry $C2/m$ (see inset in Fig. 4), as choices with higher symmetries can not index all observed intensities.

In Fig. 4, two representative neutron powder-diffraction patterns are shown, and the results of Rietveld refinements for five different temperatures are summarized in Table II. The data of Fig. 4 reveal that the sample contains about 3% of MnO as an impurity phase. This impurity phase in the neutron data probably originates from the fact that the powdered sample was exposed to air before placing it in the vanadium cup. A partial decomposition of the sample explains this minor complication in the neutron data, but there is no evidence of an antiferromagnetic ordering transition at 118 K in the magnetic investigations, which would be expected if a significant amount of MnO was present in the original single crystal as well.

According to the thermodynamic data (see above), $BaMn_2O_3$ orders magnetically at 184 K and, indeed, magnetic Bragg peaks are visible at 180 K. Simultaneously, several nuclear peaks split, indicating that the symmetry is lowered, in agreement with the lowering to the monoclinic symmetry obtained from the low-temperature single-crystal x-ray data. An example of the splitting is shown in Fig. 5(a); the two intensities, indexed as (1,5,2) ($2\Theta = 149.5°$) and (3,2,1) ($2\Theta = 150.6°$) in the centered orthorhombic setting ($Immm$), shift only slightly between 200 and 190 K, as a result of shrinkage of the unit cell, but, at 170 K, both peaks are clearly split and their intensities are distributed. At 180 K, the experimental resolution is not sufficient to resolve the peak splitting induced by the small monoclinic distortion. Because of the high scattering angle, we may safely neglect any magnetic scattering as a possible cause of the peak splitting.

The emergence of the magnetic Bragg peaks upon cooling is shown for the example of the (1,1,-1/2)/(1,-1,-1/2) reflection in Fig. 6(b). This purely magnetic intensity develops from a diffuse scattering, which is present already at 200 K as a broad hump on top of the background intensity. At 190 K, the diffuse scattering sharpens, which means that the spin-spin correlation length increases, and at 180 K, this peak exhibits a well-defined

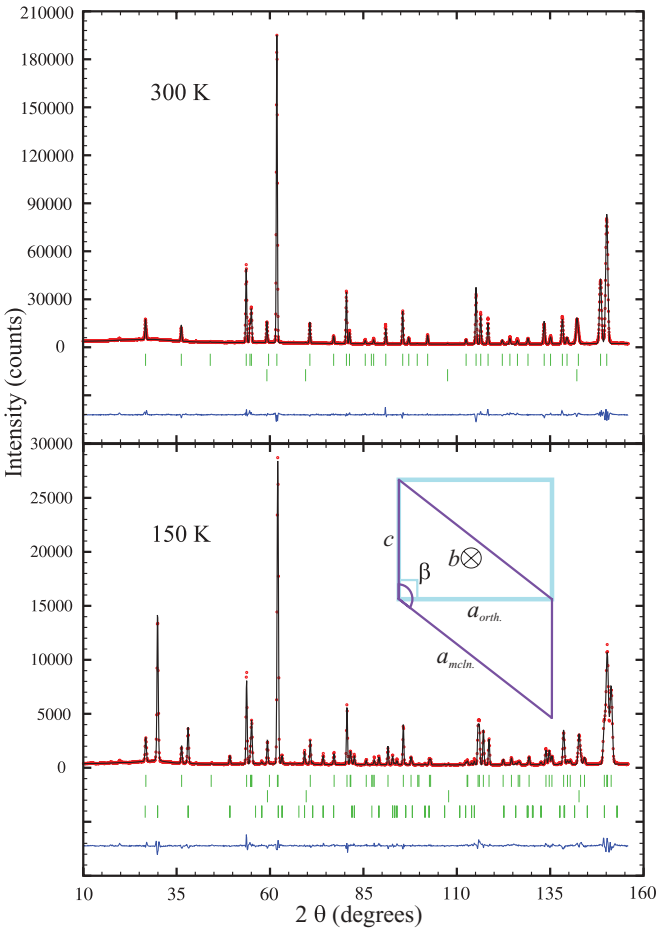

FIG. 4. (Color online) Neutron diffraction data of $BaMn_2O_3$ at 300 (top) and 150 K (bottom). Observed intensities are marked by circles and the calculated pattern as a line. All Bragg intensities are indicated by vertical lines: $BaMn_2O_3$ (1st row), MnO (2nd row), and $BaMn_2O_3$ spin structure (3rd row). The lowest line is the difference between observed and calculated intensities $I_{obs} - I_{calc}$. The inset compares the a, c planes of the orthorhombic and the monoclinic unit cells.

half-width, close to that of the nuclear scattering intensities at a similar scattering angle, e.g., $(0,2,0)_{mcln}$.

To enable unit-cell comparisons between all temperatures, the monoclinic unit cell was refined on all diffraction data, and the result is shown in Fig. 6. The lattice constants a, b, and c decrease continuously on cooling between 300 and 50 K, but a changes much stronger than b and c. A small anomaly in the a parameter is visible on cooling through T_N. As shown in the inset of Fig. 6, the monoclinic angle β indicates that the structure distorts below 180 K. Above 200 K, the value of β was fixed to the value calculated via the orthorhombic lattice constants (see inset of Fig. 4), i.e., $\beta = 90° + \arctan(\frac{c_{orth}}{a_{orth}})$. In the bottom panel of Fig. 6, we show the ordered Mn^{2+} magnetic moment as a function of temperature.

All magnetic Bragg peaks appearing below $T_N \simeq 184$ K can be indexed with the propagation vector $k = (0,0,1/2)$, i.e., by a doubling of the c axis. This means that the next-nearest-neighbor ladders connected by one c-lattice spacing are ordering antiferromagnetically, whereas spins in

TABLE I. Single-crystal x-ray data of $BaMn_2O_3$ at 150 and 100 K. All atomic positions are assumed to be fully occupied, U_{iso} and U_{ij} are given in (10^{-4} Å^2) with standard deviations in parentheses, and the cell parameters are adopted from the neutron powder-diffraction data at the same temperature.

Temperature (K)	150	100
2a Ba (x,y,z) U_{iso}	(0, 0, 0) 69(1)	(0, 0, 0) 51(1)
U_{11}, U_{22}, U_{33}, U_{12}, U_{13}, U_{23}	74(1), 69(1), 71(1), 0, 50(1), 0	57(1), 52(1), 53(1), 0, 38(1), 0
4g Mn (x,y,z) U_{iso}	(0, 0.31183(3), 0) 68(2)	(0, 0.31183(3), 0) 43(1)
U_{11}, U_{22}, U_{33}, U_{12}, U_{13}, U_{23}	68(2), 62(2), 75(2), 0, 46(1), 0	56(1), 50(1), 59(1), 0, 37(1), 0
2b O (x,y,z) U_{iso}	(0, 1/2, 0) 92(9)	(0, 1/2, 0) 75(9)
U_{11}, U_{22}, U_{33}, U_{12}, U_{13}, U_{23}	98(9), 61(7), 112(9), 0, 65(8), 0	93(9), 43(7), 94(8), 0, 61(7), 0
4h O (x,y,z) U_{iso}	(0, 0.2036(2), 1/2) 85(6)	(0, 0.2036(1), 1/2) 69(6)
U_{11}, U_{22}, U_{33}, U_{12}, U_{13}, U_{23}	76(6), 89(6), 90(6), 0, 53(5), 0	63(5), 71(5), 74(5), 0, 43(5), 0
Space group (Nr.)	$C2/m$ (12)	$C2/m$ (12)
a,b,c (Å)	5.62060(2), 10.96155(3), 3.53794(2)	5.61194(2), 10.95766(3), 3.53324(2)
α,β,γ (°)	90, 128.8199(2), 90	90, 128.7261(1), 90
S (obs, all)	1.21, 1.21	1.16, 1.17
R (obs, all)	0.0189, 0.0189	0.0175, 0.0175
R_w (obs, all)	0.0546, 0.0547	0.0518, 0.0518
Refined structure factor	F^2	F^2
Z	2	2
Transmission min/max (mm^{-1})	0.0659/0.1291	0.0980/0.1714
Absorption coefficient	18.527	18.555
$F(000)$	260	260
Reflections total	561	563
Reflections ($I > 3\sigma$)	557	561
Peak/hole (e/Å^3)	0.87/−1.24	0.95/−1.25

the next-nearest-neighbor ladders connected by one *b*-lattice spacing align parallel. The magnetic interaction along *c* is mediated by the weak J_3 parameter (see Fig. 7), which the observation of doubling along *c* determines to be antiferromagnetic. Due to the 180° Mn–O–Mn bonds, there is no doubt that the intraladder interaction parameters J_1 and J_2

TABLE II. Atomic and magnetic parameters of $BaMn_2O_3$ at different temperatures. All atomic positions are assumed to be fully occupied and the standard deviations are already multiplied by the Berar-Lelann factor (Ref. 29) and an additional factor of 3 to compensate for pronounced texture effects in the raw data (Ref. 30). Data for MnO was taken from G.R. Levi (Ref. 31) and Goodwin *et al.* (Ref. 32).

Temperature (K)	300	200	150	100	3
Ba (x,y,z)	1/2, 1/2, 0	1/2, 1/2, 0	0, 0, 0	0, 0, 0	0, 0, 0
U_{iso} (Å^2)	0.0073(5)	0.0045(4)	0.0054(7)	0.0073(6)	0.0033(9)
Mn (x,y,z)	1/2, 0.1882(1), 0	1/2, 0.18811(9), 0	0, 0.3125(9), 0	0, 0.3124(9), 0	0, 0.312(1), 0
U_{iso} (Å^2)	0.0130(5)	0.0132(4)	0.0085(7)	0.0094(7)	0.0075(9)
O1 (x,y,z)	0, 1/2, 1/2	0, 1/2, 1/2	0, 1/2, 0	0, 1/2, 0	0, 1/2, 0
U_{iso} (Å^2)	0.0190(5)	0.0172(4)	0.0116(7)	0.0127(7)	0.0144(9)
O2 (x,y,z)	0, 0.2048(1), 0	0, 0.20423(9), 0	0, 0.2039(2), 1/2	0, 0.20402(9), 1/2	0, 0.2030(1), 1/2
U_{iso} (Å^2)	0.0176(4)	0.0161(3)	0.0157(5)	0.0154(5)	0.0101(6)
Space Group (Nr.)	$Immm$ (71)	$Immm$ (71)	$C2/m$ (12)	$C2/m$ (12)	$C2/m$ (12)
a (Å)	4.3834(1)	4.38006(6)	5.62060(6)	5.61194(6)	5.60595(6)
b (Å)	10.9751(2)	10.96636(9)	10.96155(9)	10.9577(1)	10.9553(1)
c (Å)	3.5549(1)	3.54433(6)	3.53794(6)	3.53324(6)	3.53000(6)
β (°)	90	90	128.8199(3)	128.7261(3)	128.6678(3)
χ^2	4.23	2.23	8.78	4.46	5.94
R_{Bragg}	0.0572	0.0448	0.0528	0.0611	0.0723
R_F	0.0556	0.0412	0.0480	0.0454	0.0540
Magnetic k vector			[0,0,1/2]	[0,0,1/2]	[0,0,1/2]
Magnetic moment M (μ_B)			3.30(6)	4.12(3)	4.67(3)
Angle $\Phi = \angle(M,c)$ (°)			71	75	76
R_{mag}			0.120	0.101	0.095
Comment	MnO 3.13(6)%	MnO 3.09(6)%	MnO 2.94(6)%	MnO excluded	MnO excluded

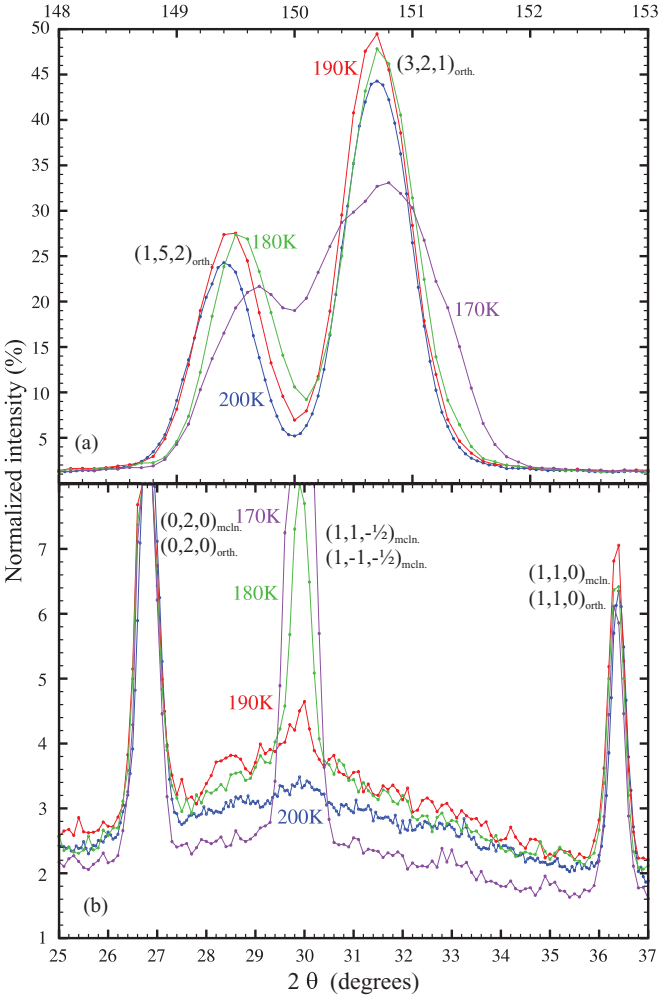

FIG. 5. (Color online) Representative neutron diffraction data at four temperatures. (a) Two of the peaks from the high-temperature orthorhombic structure are indexed and the splitting of, especially the [321] peak, is made clear. (b) The growth of the largest magnetic peak displayed at the same temperatures as in (a) and indexed according to high- and low-temperature crystallographic settings.

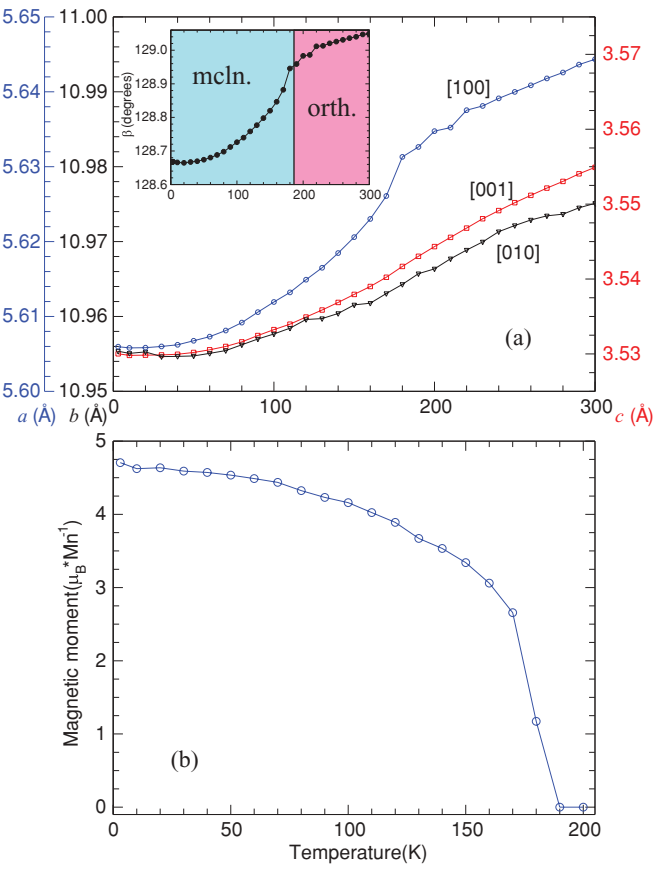

FIG. 6. (Color online) (a) The monoclinic unit-cell parameters, the β angle (inset), and (b) the ordered magnetic moment of Mn^{2+} as functions of temperature.

must be strong and antiferromagnetic, which unambiguously fixes the antiferromagnetic structure within a single ladder. The arrangement of the spins in ladders displaced by one a or by one c lattice spacing is fully determined by the propagation vector defining the magnetic translation symmetry, but the arrangement of magnetic moments between nearest-neighbor ladders connected by the body centering of the orthorhombic lattice (1/2, 1/2, 1/2) has been left open so far. However, the two choices of parallel or antiparallel alignment do not result in different symmetries, but only in two different domain types. Choosing a parallel alignment of the Mn spins at (1/2, 0.18, 0) and at (1/2, 0.18, 0) + (1/2, 1/2, 1/2) yields an antiparallel alignment for spins at (1/2, 0.18, 0) and (1/2, 0.18, 0) + (1/2, −1/2, 1/2) and *vice versa*. The magnetic symmetry constructed above is monoclinic, and the two domain types correspond to the common symmetry reduction from orthorhombic to monoclinic.

Symmetry analysis within the low-temperature space group $C2/m$ indicates that, within a single representation, spins align either in the monoclinic a, c planes or along the b axis. Since there is no indication that the magnetic transition is split, and since the magnetic transition seems to be of only weak first-order character, a single representation should be sufficient to describe the magnetic structure. Since the magnetic susceptibility clearly indicates antiferromagnetic

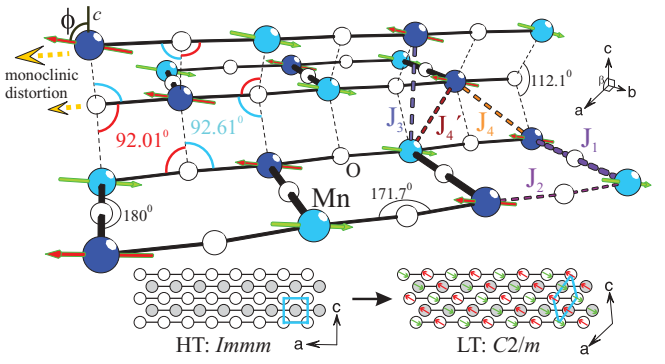

FIG. 7. (Color online) The magnetic structure of $BaMn_2O_3$ at 3 K, represented on its Mn-O sublattice. The magnetic moments of Mn are represented by arrows. The thick dashed lines represent the different Mn–to–Mn interaction parameters (J_1–J_4). The arrows on the left show the ladder shift through the monoclinic distortion, as discussed in the text. The bottom panels compare the high-temperature (HT) and low-temperature (LT) structures of $BaMn_2O_3$.

ordering with spins aligned perpendicular to the b axis, we refined the collinear magnetic structure with the spins aligned parallel to the monoclinic a,c planes. The ordered magnetic moment is fully determined by its absolute value, given in Fig. 6, and by the angle it forms with respect to the c axis, which is roughly temperature independent. Both values are given in Table II With this magnetic structure, the neutron powder-diffraction data are perfectly described. Note that the magnetic superstructure peaks are quite strong, comparable to the nuclear reflections. The Mn^{2+} ordered moment rapidly increases and half of the expected $5\mu_B$ is observed already at 170 K. With further decreasing temperature, the moment further increases and finally saturates at $\simeq 4.7\mu_B$, close to the expected value.

The role of the monoclinic structural distortion in $BaMn_2O_3$ has to be discussed concerning two aspects. First, the monoclinic distortion is just a consequence of the monoclinic magnetic symmetry, but, one would only expect a weak structural deformation. Second, the monoclinic distortion lifts the frustration of magnetic exchange interaction and thereby stabilizes the magnetic order in $BaMn_2O_3$ significantly. The nearest-neighbor interladder interaction parameters J_4 and J_4' are mediated via Mn–O–Mn bonds close to a 90° configuration; see Fig. 7. In the high-temperature phase, both Mn–O–Mn angles amount to 92.3° [Fig. 1(b)], which causes a perfect geometrical frustration. On cooling through T_N, the structure changes from orthorhombic to monoclinic and induces an antisymmetric shift of the ladders, which changes the corresponding Mn–O–Mn angles by ±0.3° and lifts the perfect geometrical frustration. According to the Goodenough-Kanamori rules,[8,9] a decreasing Mn–O–Mn angle results in a monotonic decrease from a large antiferromagnetic interaction at an 180° bond to a weak ferromagnetic coupling at a 90° bond. Thus, one might expect J_4' with the larger angle of 92.61° to be increased while J_4 with the smaller angle of 92.01° to be decreased. This is, however, in contrast to our neutron data, which clearly show that the neighboring spins connected via the larger bond angle of 92.61° are aligned parallel; see Fig. 7. This means that J_4 is larger than J_4', which most probably means that the minimum in the Mn–O–Mn angular dependence is located at a bond angle above 93°, which corresponds well to the observation in $CuGeO_3$.[33,34]

As a result of the strong sensitivity of the magnetic interaction on the Mn–O–Mn bond angle, a sizable magnetoelastic effect occurs in $BaMn_2O_3$, similar to the spin-Peierls compound $CuGeO_3$ where dimerization mainly arises from a Cu–O–Cu bond-angle modulation.[33,34] A similar lifting of geometric frustration through a coupled structural and magnetic transition has been reported recently for VOCl (Ref. 35) and seems to be relevant in the parent phase of the iron-arsenide superconductors as well. In LaOFeAs, the magnetic order is associated with a tetragonal-to-orthorhombic transition, which also has a two-fold role.[36] It is a consequence of the lower magnetic symmetry, and it lifts a magnetic frustration thereby stabilizing the magnetic order in full analogy to the discussion presented above for $BaMn_2O_3$.

V. CONCLUSIONS

We have presented a detailed study of large single crystals of $BaMn_2O_3$ grown in a floating-zone image furnace. $BaMn_2O_3$ has structural motifs from both the hexagonal $RMnO_3$ (Ref. 22) and the well-known spin-ladder compound $(Sr,Ca)_{14}Cu_{24}O_{41}$.[37] Although $BaMn_2O_3$ contains spin ladders with obvious geometrical frustration, this compound shows long-range antiferromagnetic order at $T_N \simeq 184$ K. The magnetic ordering is accompanied by a distortion of the crystal structure, which is described by a lowering of the symmetry from orthorhombic to monoclinic. Data from both specific-heat and thermal-expansion measurements clearly indicate that this phase transition shows a weak temperature hysteresis. The weak first-order feature of this magnetically driven phase transition is attributed to a strong magnetoelastic coupling. The magnetic correlations above T_N are most likely confined within the ladders, which cannot show long-range order because of the low dimensionality of the (almost) isotropic Heisenberg spin system. The low dimensionality of the magnetic subsystem of $BaMn_2O_3$ is a consequence of a very effective magnetic decoupling between neighboring spin ladders as a result of a perfect geometrical frustration. Experimentally, this low dimensionality is reflected by broad maxima in the temperature dependence of the magnetic suceptibility, which are located around 270 K, suggesting an average intraladder interaction $J \simeq 40$ K. The low dimensionality is also clearly seen in the neutron diffraction data, where pronounced short-range magnetic correlations are observed already well above T_N. The neutron data reveal that, at T_N, the magnetic correlations become long range and, in addition, there is an antisymmetric shift of neighboring spin ladders, which results in an alternation of the corresponding Mn–O–Mn angles along the ladder direction. As a consequence, the geometrical frustration is lifted, the spin ladders become three-dimensionally coupled, and, simultaneously, the magnetic subsystem develops long-range antiferromagnetic order. This indicates that the structural phase transition from orthorhombic to monoclinic in $BaMn_2O_3$ is driven by a gain in the magnetic free energy.

ACKNOWLEDGMENTS

We would like to thank Daniel Khomskii for his invaluable comments and Inge Simons for performing the elemental analyses. This work was supported by the Deutsche Forschungsgemeinschaft through Sonderforschungsbereich 608.

[1] Z. Hiroi, M. Azuma, M. Takano, and Y. Bando, J. Solid State Chem. **95**, 230 (1991).

[2] E. Dagotto, J. Riera, and D. Scalapino, Phys. Rev. B **45**, 5744 (1992).

[3] E. Dagotto and T. M. Rice, Science **271**, 618 (1996).

[4] S. R. White, I. Affleck, and D. J. Scalapino, Phys. Rev. B **65**, 165122 (2002).

[5] S. T. Carr and A. M. Tsvelik, Phys. Rev. B **65**, 195121 (2002).

[6]P. Lemmens, G. Güntherodt, and C. Gros, Phys. Rep. **375**, 1 (2003).
[7]T. Vuletic, B. Korin-Hamzic, T. Ivek, S. Tomic, B. Gorshunov, M. Dressel, and J. Akimitsu, Phys. Rep. **428**, 169 (2006).
[8]J. B. Goodenough, Phys. Rev. **100**, 564 (1955).
[9]J. Kanamori, J. Phys. Chem. Solids **10**, 87 (1959).
[10]R. S. Eccleston, M. Azuma, and M. Takano, Phys. Rev. B **53**, 14721 (1996).
[11]M. Martin-Delgado, J. Dukelsky, and G. Sierra, Phys. Lett. A **250**, 430 (1998).
[12]M. Windt *et al.*, Phys. Rev. Lett. **87**, 127002 (2001).
[13]M. Klanjšek *et al.*, Phys. Rev. Lett. **101**, 137207 (2008).
[14]Ch. Rüegg *et al.*, Phys. Rev. Lett. **101**, 247202 (2008).
[15]B. Thielemann *et al.*, Phys. Rev. Lett. **102**, 107204 (2009).
[16]A. V. Sologubenko, K. Giannò, H. R. Ott, U. Ammerahl, and A. Revcolevschi, Phys. Rev. Lett. **84**, 2714 (2000).
[17]C. Hess, C. Baumann, U. Ammerahl, B. Büchner, F. Heidrich-Meisner, W. Brenig, and A. Revcolevschi, Phys. Rev. B **64**, 184305 (2001).
[18]T. Lorenz, O. Heyer, M. Garst, F. Anfuso, A. Rosch, C. Rüegg, and K. Krämer, Phys. Rev. Lett. **100**, 067208 (2008).
[19]F. Anfuso, M. Garst, A. Rosch, O. Heyer, T. Lorenz, C. Rüegg, and K. Krämer, Phys. Rev. B **77**, 235113 (2008).
[20]K. Sander and H. K. Müller-Buschbaum, Z. Anorg. Allg. Chem. **451**, 35 (1979).
[21]V. Tangoulis, Chem. Phys. **332**, 271 (2007).
[22]J. S. Zhou, J. B. Goodenough, J. M. Gallardo Amores, E. Moran, M. A. Alario-Franco, and R. Caudillo, Phys. Rev. B **74**, 014422 (2006).
[23]L. Kihlborg and M. Israelsson, Acta Chem. Scand. **22**, 1685 (1968).
[24]J. C. Lashley *et al.*, Cryogenics **43**, 369 (2003).
[25]L. J. Dejongh and A. R. Miedema, Adv. Phys. **23**, 1 (1974).
[26]L. P. Kadanoff, W. Gotze, D. Hamblen, R. Hecht, E. A. S. Lewis, V. V. Palciauskas, M. Rayl, J. Swift, D. Aspnes, and J. Kane, Rev. Mod. Phys. **39**, 395 (1967).
[27]T. Ito, K. Ito, and M. Oka, Jpn. J. Appl. Phys. **17**, 371 (1978).
[28]J. Rodríguez-Carvajal, Phys. B **192**, 55 (1993).
[29]J. F. Berar and P. Lelann, J. Appl. Crystallogr. **24**, 1 (1991).
[30]The full two-dimensional analysis of the neutron powder data exhibited internal structure because the powder contained comparatively large grains. To correct this effect in the Rietveld refinement, we used an enhanced absorption correction and multiplied all standard deviations from the refinements by an additional factor of 3. This factor was estimated by comparing the data from the refinement with the larger absorption with those from a refinement with a correct absorption correction which, however, yields negative thermal displacements.
[31]G. R. Levi, Rend. Ist. Lomb Sci. Lett. Cl. Sci. Mat. Nat. **57**, 619 (1924).
[32]A. L. Goodwin, M. G. Tucker, M. T. Dove, and D. A. Keen, Phys. Rev. Lett. **96**, 047209 (2006).
[33]W. Geertsma and D. Khomskii, Phys. Rev. B **54**, 3011 (1996).
[34]M. Braden, G. Wilkendorf, J. Lorenzana, M. Aïn, G. J. McIntyre, M. Behruzi, G. Heger, G. Dhalenne, and A. Revcolevschi, Phys. Rev. B **54**, 1105 (1996).
[35]A. C. Komarek, T. Taetz, M. T. Fernández-Díaz, D. M. Trots, A. Möller, and M. Braden, Phys. Rev. B **79**, 104425 (2009).
[36]T. Yildirim, Phys. Rev. Lett. **101**, 057010 (2008).
[37]S. M. Kazakov, J. Karpinski, G. I. Meijer, C. Bougerol-Chaillout, and M. Nunez-Regueiro, Phys. C (Amsterdam) **351**, 301 (2001).